COHERENCE ESTIMATION FOR SAR IMAGERY

R. Touzi[*], A. Lopes[†], J. Bruniquel[‡], P. W. Vachon[*]

Abstract

In dual- or multiple-channel Synthetic Aperture Radar (SAR) imaging modes, cross-channel correlation is a potential source of information. The sample coherence magnitude is calculated over a moving window to generate a coherence magnitude map. High resolution coherence maps may be useful to discriminate fine structures. Coarser resolution is needed for a more accurate estimation of the coherence magnitude. In this study, the accuracy of coherence estimation is investigated as a function of the coherence map resolution. It is shown that the space-averaged coherence magnitude is biased towards higher values. The accuracy of the coherence magnitude estimate obtained is a function of the number of pixels averaged and the number of independent samples per pixel (i.e. the coherence map resolution). A method is proposed to remove the bias from the space-averaged sample coherence magnitude. Coherence magnitude estimation from complex (magnitude and phase) coherence maps is also considered. It is established that the magnitude of the averaged sample coherence estimate is slightly biased for high resolution coherence maps, and that the, bias reduces with coarser resolution. Finally, coherence estimation for nonstationary targets is discussed. It is shown that the averaged sample coherence obtained from complex coherence maps or coherence magnitude maps is suitable for estimation of nonstationary coherence. The averaged sample (complex) coherence permits the calculation of an unbiased coherence estimate provided that the original signals can be assumed to be locally stationary over a sufficiently coarse resolution cell.

[*]Canada Centre for Remote Sensing, 588 Booth Street, Ottawa Ontario, Canada K1A OY7
[†]CESBIO (CNES/CNRS/UPS), 18 Av. Ed. Belin 31055 Toulouse, France
[‡]Alcatel Espace, 26 Av.J.F. Champollion, 31073 Toulouse, France

Contents

LIST OF FIGURES AND TABLES

LIST OF SYMBOLS

- z_1, and z_2: zero-mean complex signals z_1 and z_2;
- Δ: actual (complex) coherence;
- $\bar{\Delta}$: actual averaged (complex) coherence;
- β: effective phase difference;
- δ: sample (complex) coherence;
- $\bar{\delta}_L$: averaged sample coherence magnitude;
- D: actual coherence magnitude;
- $\bar{D}$: actual averaged coherence magnitude;
- d: sample coherence magnitude;
- $\bar{d}_L$: averaged sample coherence magnitude;
- d^{sig}: Siegert coherence magnitude estimate;
- $\bar{d}_L^{sig}$: averaged Siegert coherence magnitude estimate;
- δ^{olk}: Olkin coherence estimate;
- $\bar{\delta}_L^{olk}$: averaged Olkin coherence estimate;
- R: actual correlation coefficient of real channels;
- r: sample correlation coefficient of real channels;
- w: textural parameter.

1 INTRODUCTION

In certain Synthetic Aperture Radar (SAR) imaging modes, such as multi-temporal interferometry and polarimetry, the radar data are presented in two or more channels. The inter-channel correlations may be used as sources of information. The magnitude of the cross-channel correlation coefficient, called the coherence magnitude (or the degree of coherence) [1], is calculated to generate a coherence (magnitude) map [23] which can be used for target classification [3, 11, 26]. In interferometry, the coherence magnitude map is generated to select areas in which the "coherent" phase may be processed to extract information about target elevation or target displacement. For example, the topography in boreal forest areas can be estimated only for areas where the coherence magnitude is larger than about 0.2 [11]. The local precision of a digital elevation model generated from a repeat-pass SAR interferogram depends on the coherence magnitude [11, 16]. The coherence also may be required to calculate the effective number of looks [26], or to measure the signal-to-noise ratio for a given system [4]. Quantitative coherence information is very important in many applications, and as such, the coherence should be estimated accurately.

In this paper, various methods, as summarized in Figure 1, are investigated for unbiased estimation of the coherence magnitude.

In Section 2, the sample coherence magnitude, which is frequently used to estimate the cross-channel coherence magnitude, is considered. Its statistics are derived for Gaussian scenes, and are extended to non-Gaussian scenes. The estimate is shown to be significantly biased under low coherence conditions, and the possibility of deriving an unbiased estimate is investigated. The use of the Siegert relationship for coherence magnitude estimation is also discussed.

In Section 3, estimation of coherence magnitude from coherence magnitude maps is considered. It is shown that the averaged sample coherence magnitude is biased towards higher values. The statistics of the sample coherence magnitude are used to remove the coherence estimate bias, and to calculate the precision of the estimate as a function of the number of looks L contained in each sample (i.e resolution coherence map), and the number N of averaged pixels (sample coherence magnitude). The method is validated using actual SAR data, and the results are extended to non-Gaussian scenes.

In Section 4, coherence magnitude estimation from (complex) coherence maps is discussed. The coherence is calculated over a moving window, and the complex value is assigned to the map pixel at the corresponding spatial position. The magnitude of the space-averaged sample (complex) coherence is investigated as a candidate for coherence magnitude estimation. To assess the accuracy of the estimate, the statistics of the sample coherence are derived for Gaussian areas. It is established that the magnitude of the averaged sample coherence estimate is slightly biased for high resolution coherence maps, and that the bias reduces with coarser resolution. For high resolution coherence maps, the statistics of the sample coherence are used to remove the bias estimate. An unbiased coherence estimate is also introduced for a

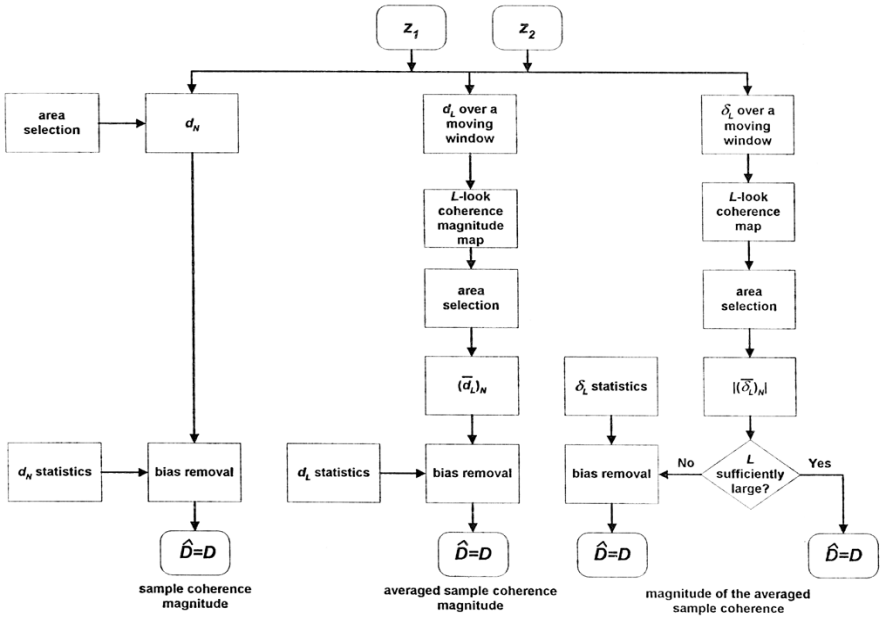

(a)

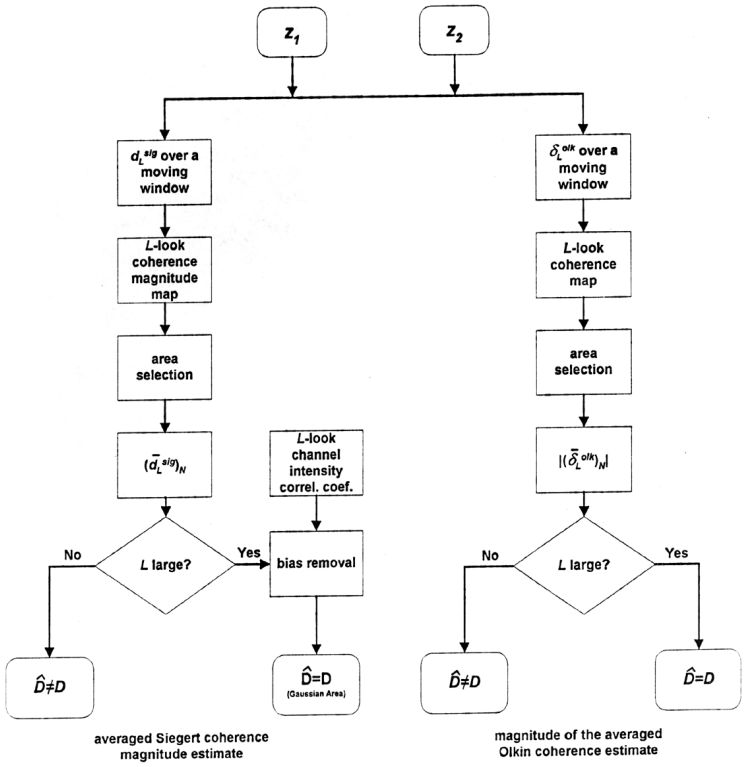

(b)

Figure 1: Method diagram for unbiased coherence magnitude estimation. (a) General methods and (b) methods for jointly circular Gaussian distributed channels.

jointly circular complex Gaussian process.

Estimation of coherence for nonstationary processes is investigated in Section 5. The averaged coherence is defined to characterize nonstationary coherence signals. Under a local stationarity assumption, the averaged coherence can be estimated using the space-averaged sample coherence obtained from coherence magnitude maps or complex coherence maps. The accuracy of the estimate obtained is discussed as a function of the resolution map. Implications for the estimation in SAR interferometry of the topographic phase corrected coherence are then explored. Finally, examples of coherence magnitude estimation are illustrated in Section 6, using CCRS Convair 580 polarimetric SAR data.

2 THE SAMPLE COHERENCE MAGNITUDE FOR COHERENCE MAGNITUDE ESTIMATION

2.1 Coherence magnitude estimate

The complex coherence of two zero-mean complex signals z_1 and z_2 is defined in [1] for (wide-sense) stationary processes as the channel correlation coefficient for zero time shift:

$$\Delta = \Delta(0) = \frac{E(z_1 z_2^*)}{\sqrt{E(|z_1|^2)}\sqrt{E(|z_2|^2)}}, \tag{1}$$

where $E(x)$ is the expected value of x. The coherence magnitude $D = |\Delta|$ is called the degree of coherence, and the argument of Δ is the effective phase difference. Under the assumption that the processes involved in equation (1) are also ergodic (in mean), the sample coherence δ is frequently used as the coherence estimate $\delta = \hat{\Delta}$. Given L signal measurements, the sample coherence δ is:

$$\delta = \frac{\sum_{i=1}^{L} z_{1i} z_{2i}^*}{\sqrt{\sum_{i=1}^{L} |z_{1i}|^2}\sqrt{\sum_{i=1}^{L} |z_{2i}|^2}}, \tag{2}$$

where i is the sample number. The coherence magnitude estimate $d = \hat{D}$ can be deduced as:

$$d = |\delta| \tag{3}$$

If the coherence expression (1) is reconsidered, it can be noted that z_1 and z_2 which are assumed to be stationary, are also jointly stationary. Stationarity of the processes (z_1, z_2, and $z_1 z_2^*$) involved in equation (1) is required such that the time averages of each process converge to a finite limit. Ergodicity in mean is also required so that the different time averages of each process converge to the same limit: the ensemble average. The ensemble averages can then be substituted in equation (1) with the time averages, and the sample coherence of equation (2) provides a coherence estimate which should be asymptotically unbiased.

In the following (Sections 2, 3, and 4), the processes involved in equation (1) are assumed to be ergodic in mean, and the coherence will be estimated in areas named "stationary" in which the channels z_1 and z_2 are stationary and jointly stationary. Coherence estimation in nonstationary scenes will be discussed in Section 5.

2.2 Statistics of the sample coherence magnitude within Gaussian scenes

2.2.1 Pdf and moments

The sample coherence magnitude d is the Maximum Likelihood (ML) estimate of the coherence magnitude D. An analytical expression for its probability density function (pdf) was derived in [31] for a jointly complex Gaussian process (z_1, z_2) as a function of the coherence magnitude D, the number L of integrated independent samples ($L > 2$), and the hypergeometric function F:

$$p_d(d|D) = 2(L-1)(1-D^2)^L d(1-d^2)^{L-2} F(L, L; 1; D^2 d^2) \tag{4}$$

Notice that the pdf expression does not depend on the variances ($\sigma_i^2 = E(|z_i|^2)$ for $i = 1, 2$) of the zero mean complex processes z_1 and z_2. Equation (4) can be used to deduce the moments of order k:

$$m_k = \frac{\Gamma(L)\Gamma(1+k/2)}{\Gamma(L+k/2)} \cdot {}_3F_2(1+k/2, L, L; L+k/2, 1; D^2)(1-D^2)^L \tag{5}$$

where ${}_pF_q$ is the generalized hypergeometric function [7]. It can be shown that $m_0 = 1$, as expected.

2.2.2 Bias in the sample coherence magnitude d

An analytical expression of the first moment of d, $E(d)$, was first derived in [31]:

$$E(d) = \frac{\Gamma(L)\Gamma(1+1/2)}{\Gamma(L+1/2)} \cdot {}_3F_2(3/2, L, L; L+1/2; 1; D^2)(1-D^2)^L \tag{6}$$

Figure 2 presents $E(d)$ as a function of the coherence magnitude D.

Similar curves were obtained in [8, 10] using simulations. It can be seen that the sample coherence magnitude d is biased towards higher values, with a resulting reduction of contrast, especially between areas of differing low coherence. The bias decreases with increasing number of independent samples L as the ML estimate is asymptotically unbiased.

2.2.3 Variance of the sample coherence magnitude d

The variance of d might be needed to assess the estimate precision. Its expression is given by:

$$var(d) = E(d^2) - E(d)^2 \tag{7}$$

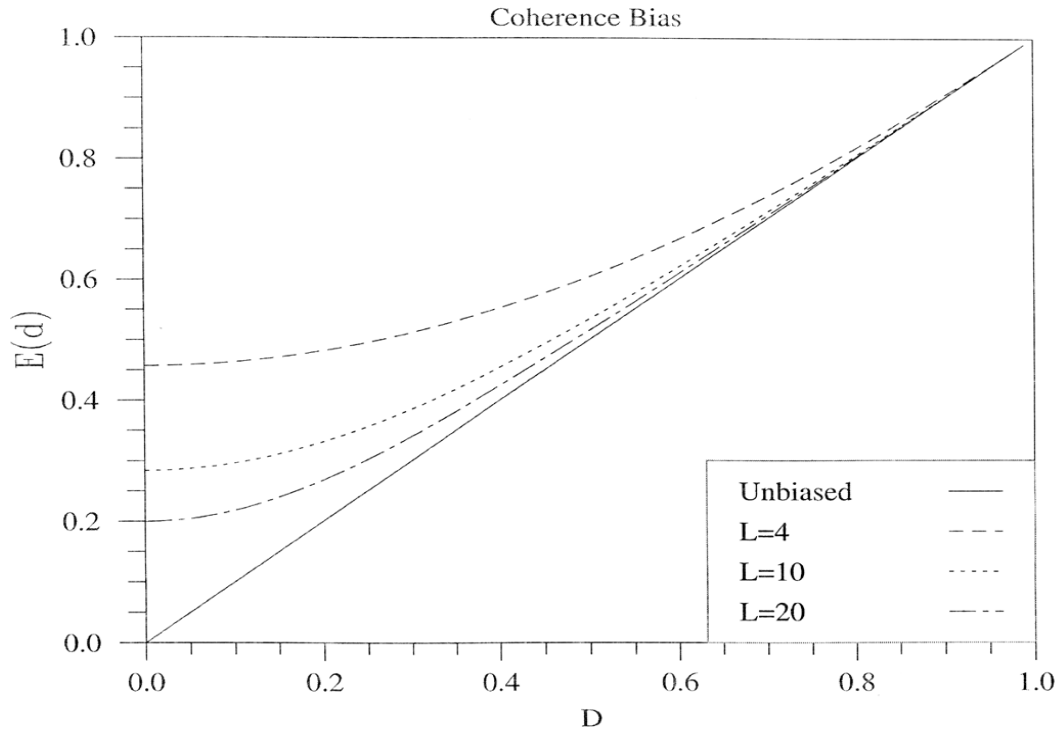

Figure 2: Coherence magnitude bias for various number of statistically independent looks.

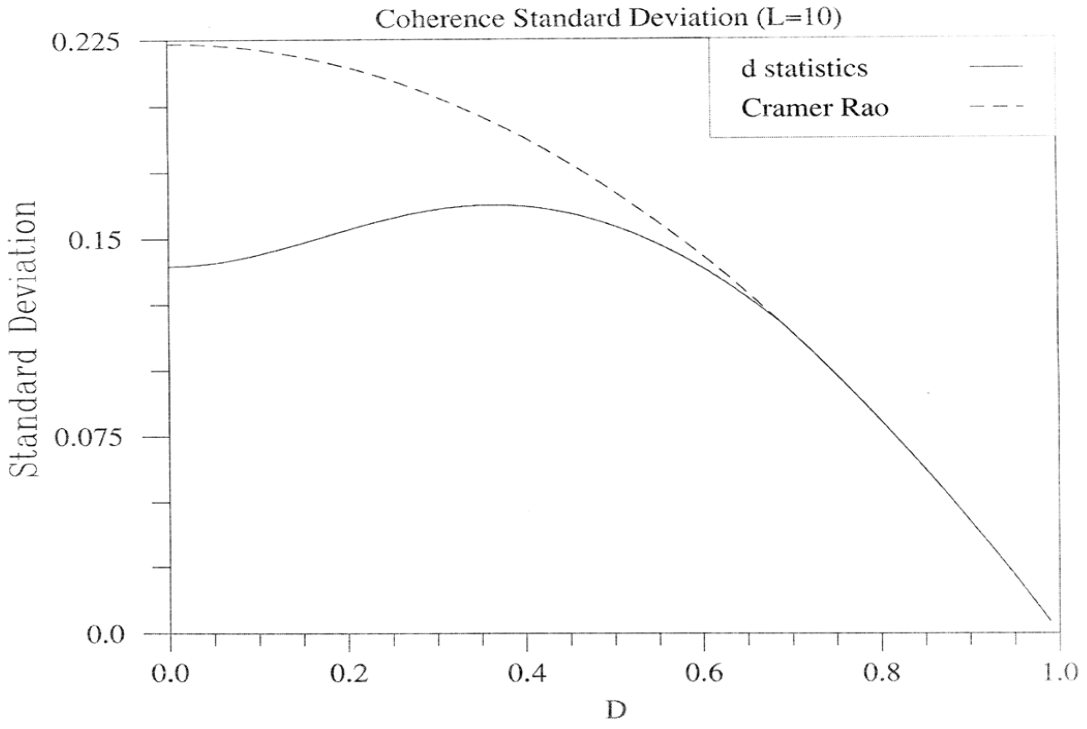

Figure 3: Standard deviation of the coherence estimate (L=10)

where $E(d^2)$ is derived from equation (5) ($k = 2$), and $E(d)$ is given by equation (6). The expression obtained may be compared numerically to the Cramer Rao (CR) lower bound var_{CR} derived in [14, 27]. Thus,

$$var_{CR} = \frac{(1 - D^2)^2}{2L} \leq var(d) \tag{8}$$

which applies only to unbiased estimates of D. Figure 3 presents the standard deviation and the square root of the CR lower bound for $L = 10$. As can be seen, the results are similar as long as the estimate is unbiased. When the estimate is biased, the expression obtained from equation (7) gives lower values than is obtained with the CR expression.

Hence, the variance expression of equation (7), which is more general than the CR lower bound, should be used for error bar calculation. If the bias can be removed, the CR lower bound var_{CR} which is more computationally efficient, can be used. The bias on the estimate should first be calculated and removed. Then the estimate obtained can be inserted in var_{CR} of equation (8) to calculate the estimate precision.

2.3 Extension of the statistics to non-Gaussian distributions

The statistics derived for Gaussian scenes can be extended to K-distributed scenes, as was done in [12, 33]. Under the assumption that the scene backscattering satisfies the product model introduced in [19], the underlying cross section variations were assumed to be due to fluctuating numbers of scatterers per resolution cell. A target textural parameter w was defined in [12, 33] as the ratio of the number N of scatterers per resolution cell to the scatterer number average $< N >$ (calculated over all the resolution cells contained in the area under study): $w = N/ < N >$. The product model assumes that the textural parameter w has the same value for the channels considered. Consequently, the fluctuations that give rise to the K-distribution cancel out when the coherence is estimated, and the coherence statistics for K-distributed areas are identical to the ones derived for Gaussian areas. The statistics can be extended to other distributions (than the K-distribution), provided that scene backscattering satisfies the product model.

In the following, all the results will be derived for Gaussian scenes, and will be extended to non-Gaussian scenes under the product model conditions.

2.4 Investigation of the function $G(d)$ for unbiased coherence estimation

One can show directly that an unbiased estimator $G(d)$, which is a function of the sample coherence magnitude d, cannot be found. We proceed in the same way as [20]. If $G(d)$ is unbiased, then $E[G(d)] = D$. Using equation (4) and the series transformation of the hypergeometric function, the unbiased condition

can be shown to be equivalent to:

$$\frac{2(L-1)}{\Gamma(L)^2}\sum_{k=0}^{+\infty}\frac{\Gamma(L+k)^2}{\Gamma(1+k)^2}\cdot A(k)\cdot D^{2k} = D(1-D^2)^{-L} \cdot \sum_{j=0}^{+\infty}\frac{\Gamma(L+j)}{\Gamma(L)\Gamma(1+j)}\cdot D^{2j+1} \quad (9)$$

where $A(k)$ is given by:

$$A(k)=\int_0^1 G(u)u^{2k+1}(1-u^2)^{L-2}\,du \quad (10)$$

This leads to a power series in D which has to be solved for any D value between 0 and 1. The problem has no solution since $G(d)$ does not depend on D. This is because the power series on the left hand side of equation (9), which involves the unknowns $A(k)$, includes only even powers of D, while the power series on the right hand side is a function of odd powers of D.

One might think that the problem could be solved for the squared sample coherence magnitude $\rho = d^2$. In this case, both power series on the right- and left-hand sides of equation equivalent to (9) would include only even powers of D, and the equation obtained might be solved in terms of the unknown $G(\rho)$. The pdf of ρ is derived from the pdf of d by a simple change of variables. The condition for an unbiased estimate i.e. $E[G(\rho)] = D^2$, leads to:

$$\frac{L-1}{\Gamma(L)^2}\sum_{k=0}^{+\infty}\frac{\Gamma(L+k)^2}{\Gamma(1+k)^2}\cdot B(k)\cdot D^{2k} = \sum_{j=0}^{+\infty}\frac{\Gamma(L+j)}{\Gamma(L)\Gamma(1+j)}\cdot D^{2j+2} \quad (11)$$

where $B(k)$ is given by:

$$B(k)=\int_0^1 G(\rho)\rho^k(1-\rho)^{L-2}\,d\rho \quad (12)$$

This equality must be satisfied for any D between 0 and 1. The coefficients of the power series on the right-hand side should be equal to those on the left-hand side of equation (11). This leads to the following set of equations with unknown $G(\rho)$:

$$\int_0^1 G(\rho)(1-\rho)^{L-2}d\rho = 0 \quad (13)$$

and

$$\int_0^1 G(\rho)\rho^{j+1}(1-\rho)^{L-2}d\rho = \frac{\Gamma(L)\Gamma(j+2)^2\Gamma(L+j)}{(L-1)\Gamma(L+j+1)^2\Gamma(j+1)} \quad (14)$$

Equation (13) can be solved only if $G(\rho)$ takes negative values, but that is not possible. Therefore, it is not possible to derive an unbiased estimator $G(\rho)$ which is a function of the squared sample coherence magnitude $\rho = d^2$.

Further, one might hope that an unbiased coherence magnitude estimate could be derived under the more restrictive condition of jointly circular complex Gaussian distributed channels. The coherence magnitude D ($D = |\Delta|$, Δ of equation (1)) can be deduced from the correlation coefficient R of the channel intensities $I_1 = |z_1|^2$ and $I_2 = |z_2|^2$ using the Siegert relationship [28]:

$$\frac{E[|z_1|^2|z_2|^2]}{E[|z_1|^2]E[|z_2|^2]} = 1 + \frac{|E[z_1 z_2]|^2}{E[|z_1|^2]E[|z_2|^2]} \tag{15}$$

which leads to [6]:

$$D^2 = R \tag{16}$$

where R is given by:

$$R = \frac{E(I_1 I_2) - E(I_1)E(I_2)}{\sqrt{E(I_1^2) - E(I_1)^2}\sqrt{E(I_2^2) - E(I_2)^2}} \tag{17}$$

An equivalent equation can be derived as a function of the sample coherence magnitude $d = \hat{D}$, and the sample correlation coefficient $r = \hat{R}$:

$$d^2 = r \tag{18}$$

where r is the sample correlation coefficient of I_1 and I_2:

$$r = \frac{< I_1 I_2 > - < I_1 >< I_2 >}{\sqrt{\langle I_1^2 - < I_1^2 > \rangle}\sqrt{\langle I_2^2 - < I_2^2 > \rangle}} \tag{19}$$

with $< I >= \frac{1}{L}\sum_{i=1}^{L} I_i$, and where i is the sample number.

The coherence magnitude estimate derived from equation (18), which is denoted d^{sig}, will be called the Siegert coherence magnitude estimate. Notice that in [8], the moments involved in equation (17) were not centered, and a different expression was obtained for the Siegert estimate. The Siegert estimate is currently used for coherence magnitude estimation from channel intensities even when channel phase is available [8, 15, 26]. Unfortunately, since the sample correlation coefficient r of real channels is biased, as was shown in [14, 20], the Siegert coherence estimate must also be biased. The statistics of r derived in [5, 14] can be used to derive the analytical expression of the estimate expectation $E(d^{sig})$, and the bias on the estimate. This bias was obtained in [8] using simulations. Like the sample coherence magnitude d, d^{sig} is biased towards higher values with a significant bias under low coherence conditions.

It is worthwhile noting that the Siegert relationship of equation (15) was established for jointly circular Gaussian distributed channels. In textured areas, equation (16) does not hold ($R^2 \neq D$), and different expressions equivalent to (16) were derived in [24, 26] as a function of the statistics of the texture random variable w (defined in Section 2.3), for scenes whose backscattering satisfy the product model. In this case, d^{sig} is not an estimate of D, and d^{sig} would lead to different results than d, even in areas of high coherence values for which the two estimates are unbiased. This result was confirmed in [26] using d^{sig} and

d coherence maps generated from ERS-1 repeat-pass data. The ratio of the two estimates was proposed in [24] as a tool to test whether an area is Gaussian.

In summary, it is not possible to derive from the sample coherence magnitude d an unbiased estimator of D. However, there is an alternative approach, as explained below.

2.5 Bias removal and confidence interval

Using equation (3), an estimate of the coherence magnitude d_N is obtained over an area which contains N independent samples. The issue here is to extract from the observation d_N an unbiased estimate of the coherence magnitude D, and to calculate the associated precision.

For a large number N of independent samples, the variance of d is low, and the probability distribution of $d = d_N$ is tightly concentrated around $E(d)$: $d_N \simeq E(d)$. Since $E(d)$ is related to the coherence magnitude D according to equation (6) ($E(d) = Func(D)$), an unbiased estimate can be obtained by inverting the equation at $E(d) = d_N$:

$$\hat{D} = Func^{-1}(E(d) = d_N) \tag{20}$$

where $Func$ is defined by equation (6).

If N is not sufficiently large, the estimate dispersion is significant (i.e. $d_N \neq E(d)$), and the method above cannot be applied. The Bayesian approach used in [4] for bias removal of the sample correlation coefficient (of channel power spectra) may be adapted to the sample coherence magnitude d using the pdf of equation (4). Under the assumption that the *a priori* probability of occurrence of D is uniform, the Maximum *a Posteriori* (MAP) estimate of D given the observed sample magnitude coherence d_N can be obtained by maximizing, with respect to D, the *posterior* density function defined in [4]:

$$h(D|\ d_N) \quad = \quad \frac{p_d(d_N|D)}{\int_0^1 p_d(d_N|D)dD} \tag{21}$$

where p_d is from equation (4). The Maximum Likelihood estimate $\hat{D}$ of the coherence magnitude D is that value of D for which $h(D|d_N)$ is a maximum. The *posterior* density function of equation (21) can then be integrated to determine the associated confidence interval for a given confidence level $P(a, b)$, where $P(a, b)$ is the *posterior* probability that D lies in the interval $[\hat{D} - a, \hat{D} + b]$.

The two methods are presented in Figure 1 (a) as the "sample coherence magnitude" methods.

3 COHERENCE MAGNITUDE ESTIMATION FROM A COHERENCE MAGNITUDE MAP

3.1 Background

In interferometry, the two original complex channels z_1 and z_2 are combined to form different multi-look products such as the interferogram (L-look coherence phase map) and the L-look coherence magnitude map. Each pixel value of the L-look coherence magnitude map corresponds to the sample coherence magnitude d_L calculated over L independent samples. The pixel values are averaged within the area of interest to provide an estimate of D. As the estimate is biased, maps of coarse resolution (i.e L of large value) are generally used to reduce the bias, and the areas of low coherence for which the estimate is significantly biased are disregarded. For example, in a study of ERS-1 SAR data, Hagberg *et al.* [11] selected areas for which the coherence $D > 0.4$. Coherence magnitude maps with $L \simeq 32$ were then generated to achieve an unbiased coherence estimate in the selected areas. The L value ($L \simeq 32$) was obtained by comparing the speckle covariance function measured from the data to the theoretical expression for the ERS-1 impulse response [9].

A method is proposed in the following for an unbiased estimation of the coherence magnitude, even under low coherence conditions. The method is then validated using actual SAR data.

3.2 Bias removal and confidence interval

Coherence magnitude may be estimated from an L-look coherence magnitude map by spatially averaging the sample coherence magnitude values over the area of interest:

$$\hat{D} = \bar{d}_L = \frac{1}{N}\sum_{i=1}^{N} d_{Li} \tag{22}$$

where d_L is the L-look sample coherence magnitude, i is the sample number, and N is the number of averaged samples. Under the assumption that the original signals are stationary and ergodic (in mean) in the area of interest, the spatial average $\bar{d}_L$ provides an unbiased estimate of the ensemble average $E(d_L)$. If a sufficiently large number N of independent L-look samples are averaged, $\bar{d}_L$ tends to be distributed normally about $E(d_L)$ with variance $var(E(d_L))/N$ ($var(E(d_L))$ from equation (7)), which decreases as N increases. $E(d_L)$ can be substituted with its ML estimate $\bar{d}_L$ in equation (6) which is inverted according to equation(20) to deduce an unbiased coherence magnitude estimate $\hat{D}$. Tables of inversion might be calculated first using equation(6) to reduce computing time. The unbiased estimate obtained is used in equation (8) to calculate the Cramer Rao lower bound var_{CR} value. The estimate confidence interval CI can then be determined as:

$$CI = [\hat{D} - z_c\sqrt{var_{CR}(\hat{D})}/\sqrt{N}, \hat{D} + z_c\sqrt{var_{CR}(\hat{D})}/\sqrt{N}] \,, \tag{23}$$

for a given confidence level fixed by the confidence coefficient value z_c. This scheme is represented in Figure 1 (a) as the "averaged sample coherence magnitude" method. The method can be extended to non-Gaussian scenes whose backscattering "locally" satisfies the product model. In this case, the textural parameter w (defined in Section 2.3) should have the same value for the channels considered at each (L-look) pixel averaged in the coherence estimate.

3.3 Validation based on actual SAR data

Assuming negligible additive noise, the speckle covariance function calculated from a complex SAR image within a homogeneous area is equivalent to the system autocorrelation function [18, 25]. Since the normalized system autocorrelation function has values between zero and one, an estimate of the normalized speckle covariance function may provide a valuable tool to assess the accuracy of coherence estimates for all possible coherence values ($0 \leq d \leq 1$) [9, 26].

As an example of this principle, consider a 1-look complex image acquired by the Canada Centre of Remote Sensing (CCRS) Convair-580 X-band SAR [17]. Sub-pixel offsets with increments of 0.1 pixel up to three pixels were generated in the azimuth direction. A bare, flat field containing about N=1000 independent samples was selected. Equation (3) was first used to calculate the sample coherence magnitude d_N over the whole area for each offset. An L-look ($L \simeq 4$) coherence magnitude map was then generated for each offset using a moving 3x3 window. The coherence magnitude estimate $\bar{d}_4$ was obtained by averaging the 4-look coherence magnitude samples over the selected area. Since the number N of independent L-look samples ($N = 1000$) was large, the variance values of the estimates d_N and $\bar{d}_4$ were low, and the estimates were assumed to be equal to their expectations (i.e $d_N \simeq E(d_N)$, and $\bar{d}_4 \simeq E(d_4)$).

Figure 4 presents, as a function of the sub-pixel offset, the speckle covariance functions obtained with the sample coherence magnitude d_N and the averaged 4-look sample coherence magnitude $\bar{d}_4$. The solid curve, which corresponds to $\bar{d}_4$, is highly biased, except for large coherence magnitude D values. $E(d_4)$ was substituted with $\bar{d}_4$ in equation (6), which was then inverted according to equation (20) to deduce the unbiased coherence magnitude presented in the same figure. Notice that the sample coherence magnitude d_N is virtually identical to the unbiased averaged sample coherence magnitude for a wide range of coherence magnitude values (as $d_N \simeq D$ for N large). For coherence magnitude values lower than 0.1, d_N becomes slightly different from the unbiased averaged 4-look coherence magnitude. This is due to the sample coherence magnitude d_N being biased for D lower than 0.1, even for a large number of independent samples ($N = 1000$). This can be checked using equation (6), which also could be used to remove the bias.

In summary, the theoretical statistics derived above for the sample coherence magnitude and for the

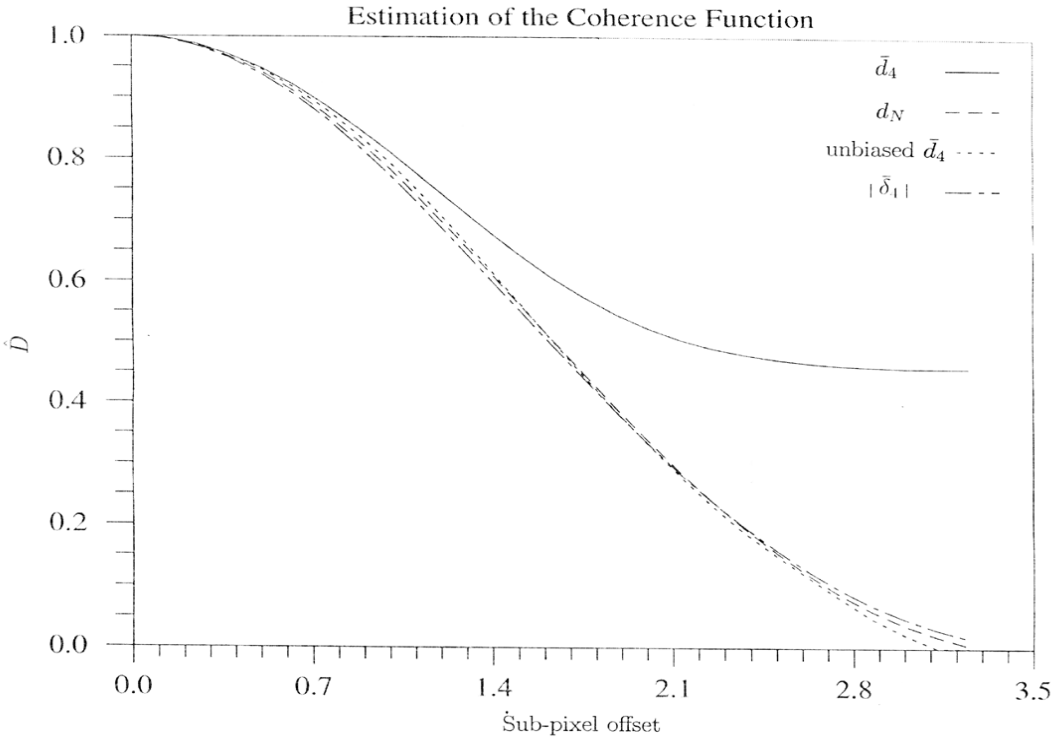

Figure 4: Estimation of the speckle covariance function.

averaged sample coherence magnitude are in agreement with the experimental results obtained from actual SAR data. The results can be extended to non-Gaussian scenes whose backscattering satisfies the product models. The averaged sample coherence magnitude method was used in [32] to provide unbiased coherence magnitude estimates which were obtained from a 20-look coherence map over Gaussian and K-distributed scenes in ERS-1 data.

3.4 The averaged Siegert coherence magnitude estimate for a joint circular Gaussian process

An estimate of the coherence magnitude D can be obtained for jointly circular Gaussian distributed channels by spatially averaging the L-look Siegert coherence magnitude samples d_L^{sig} of equation (18) over the region of interest. The coherence magnitude estimate obtained $\bar{d}_L^{sig}$ is included in Figure 1 (b) as the "averaged Siegert coherence magnitude estimate". Since the estimate d_L^{sig} is biased, $\bar{d}_L^{sig}$ is biased and a method similar to the one presented in Section 3.2, which takes into account the statistics of d_L^{sig} given in [5], may be applied to remove the bias. After bias removal, the CR lower band var_{CR} can be calculated to assess the estimate precision, as was done in Section 3.2.

Notice that the estimate bias can also be removed for non-Gaussian scenes whose backscattering satisfies

the product model. Unfortunately, the unbiased estimate obtained is not the required coherence magnitude D in the presence of texture, as shown in Section 2.4: $\bar{d}_L^{sig} = \hat{\sqrt{R}} \neq \hat{D}$ (R is from equation (17)).

4 COHERENCE ESTIMATION FROM A (COMPLEX) COHERENCE MAP

4.1 Principle

In interferometry, the multi-look channel phase difference is stored along with the multi-look sample coherence magnitude. This phase difference is the argument of the L-look sample (complex) coherence. Like the sample coherence magnitude, the sample coherence phase (L-look phase estimate) is biased [12, 29, 31]. This might be due to the spatial averaging performed during the estimation process being applied separately to the phase map and to the magnitude map. In the following, spatial averaging is done using both the magnitude and phase of L-look sample (complex) coherence, and the magnitude of the averaged L-look sample coherence is investigated as a candidate for coherence magnitude estimation.

The complex coherence $\Delta = D\exp(j\beta)$ of equation (1) may be estimated from an L-look (complex) coherence map by spatial averaging the pixel values (L-look sample coherence) over the area under study:

$$\hat{\Delta} \;=\; \bar{\delta}_L \;\;=\;\; \frac{1}{N}\sum_{i=1}^{N}\delta_{Li} \tag{24}$$

where δ_{Li} is the L-look coherence sample of equation(2), i is the sample number, and N is the number of averaged coherence samples. The magnitude of the averaged L-look sample coherence provides an estimate of the coherence magnitude $\hat{D} = |\bar{\delta}_L|$, and the argument of $\bar{\delta}_L$ is the estimate of the coherence phase β.

Under the assumption that the original signals are stationary and ergodic (in mean) in the area of interest, the spatial average $\bar{\delta}_L$ provides an unbiased estimate of $E(\delta_L)$. If a sufficiently large number N of independent L-look samples are averaged, $\bar{\delta}_L$ tends to be normally distributed (in complex) about $E(\delta_L)$. $\bar{\delta}_L$ provides the ML estimate of $E(\delta_L)$ with a precision ($var[\delta_L]/N$) fixed by the variance of δ_L, and the number N of averaged pixels. Therefore, the accuracy and the precision of the coherence estimate $\bar{\delta}_L$, and consequently of $\hat{D}$, depend on those of the sample coherence.

In the following, the statistics of the sample coherence δ of equation (2) are derived as a function of the number L of integrated independent samples. The possibility of deriving an unbiased estimate $G(\delta)$ is also discussed, and an unbiased estimate is derived under the joint circular Gaussian assumption. The results obtained will be used in Section 4.3 to assess the accuracy and the precision of the averaged sample coherence obtained from a complex coherence map.

4.2 The sample coherence for coherence estimation

4.2.1 Statistics of the sample coherence δ for Gaussian areas

Using the Wishart distribution for complex Gaussian processes, the joint pdf of the amplitude and phase (d, ϕ) of the sample coherence $\delta = d\exp(j\phi)$ (of equation (2)) is derived in Appendix 1. It is used in Appendix 2 to establish the following expression for the expectation of the sample coherence $E(\delta)$ as a function of the number of independent samples L, the coherence $\Delta = D\exp(j\beta)$ parameters D and β, and the hypergeometric function F:

$$\begin{aligned} E(\delta) &= \frac{\Gamma^2(L+1/2)}{\Gamma(L)\Gamma(L+1)} D(1-D^2)^L \exp(j\beta) \\ &\quad \cdot F(L+1/2, L+1/2; L+1; D^2) \end{aligned} \tag{25}$$

The variance of δ might be deduced using equation (25), and the 2^{nd} moment of d (from equation (5)), as follows:

$$var(\delta) = E(d^2) - |E(\delta)|^2 \tag{26}$$

Notice that the statistics of δ do not depend on the variances ($\sigma_i^2 = E(|z_i|^2)$, for $i = 1, 2$) of the zero mean complex processes z_1 and z_2, as was the case for the statistics of the sample coherence magnitude d. From equation (25), note that the coherence phase, estimated as the argument of the integrated coherence $E(\delta)$, is unbiased: $Arg[E(\delta)] = \beta$. The magnitude of the integrated coherence is, however, biased. Its bias is given by the magnitude of equation (25) as a function of the number of integrated independent samples L. $|E(\delta)|$ is presented in Figure 5 as a function of the coherence magnitude D, for different values of L. Two points can be noted concerning the bias on $|E(\delta)|$:

- it is smaller than the bias on the sample coherence magnitude d presented in Figure 2;
- it decreases very rapidly with increasing L, and becomes practically insignificant for sufficiently large (but still quite small) L ($L \geq 20$, say). For the same L value (i.e. $L = 20$), the averaged sample coherence magnitude is significantly biased for low coherence areas, as can be seen in Figure 2.

The statistics of the sample coherence δ derived for Gaussian scenes can be extended to non-Gaussian scenes which satisfy the product model, as was done in Section 2.3.

4.2.2 Investigation of the function $G(\delta)$ for unbiased coherence estimation

The same method applied in Section 2.4 can be used to investigate the function $G(\delta)$ for an unbiased estimation of the coherence. Under the assumption that the two channel processes, z_1 and z_2, obey a jointly zero mean complex Gaussian distribution, we obtain, using the statistics of the sample coherence, a double

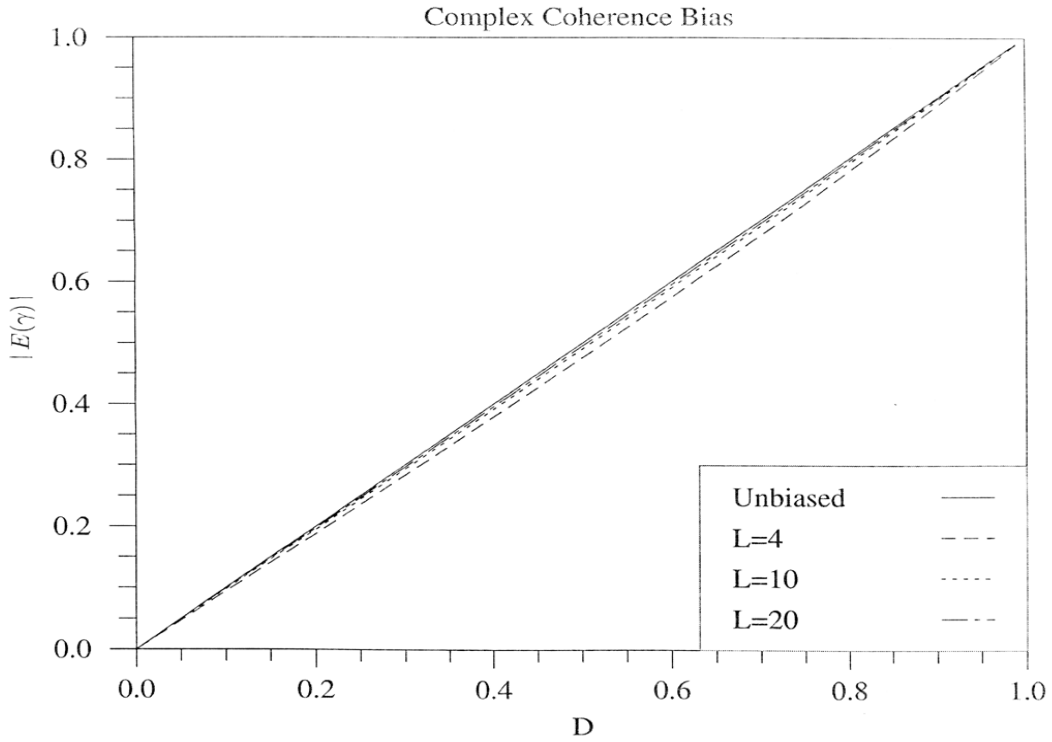

Figure 5: Coherence magnitude estimation using the averaged Siegert coherence magnitude estimate.

integral over the two parameters d and ϕ, which could not be reformulated as an analytical expression as a function of the sample coherence $\delta = d\exp(j\phi)$.

An unbiased coherence estimate may be derived if the channel complex signals were assumed to be jointly circular complex Gaussian distributed. This means that, in addition to the joint Gaussian assumption made above, the zero mean complex channels z_1 and z_2 have to satisfy the following conditions [6]:

$$\begin{aligned} E[I_k I_l] &= E[Q_k Q_l] \\ E[I_k Q_l] &= -E[I_l Q_k] \end{aligned} \tag{27}$$

where I_k and Q_k are the real and imaginary parts of z_k (for $k = 1, 2$). The coherence sample δ can be expressed as a function of the sample correlation coefficient of the real and imaginary components of the two channels [6, 15] :

$$\delta = r_{I_1 I_2} - j r_{I_1 Q_2} = r_{Q_1 Q_2} - j r_{I_1 Q_2} \tag{28}$$

$$\delta = r_{I_1 I_2} + j r_{I_2 Q_1} = r_{Q_1 Q_2} + j r_{I_2 Q_1} \tag{29}$$

where r_{XY} is the sample correlation coefficient r of equation (19) of two (real) channels X and Y. However,

since the sample correlation coefficient r is biased as shown in [20], the coherence estimate of equations (28), and (29) is biased. Olkin and Pratt proposed for a jointly Gaussian process an unbiased estimate $G(r)$ which can be deduced from the sample correlation coefficient r [20]. The unbiased estimate $G(r)$ was expressed as a function of the number N of independent samples, and the hypergeometric function by:

$$G(r) \;=\; rF(1/2, 1/2; (N-1)/2; 1-r^2) \tag{30}$$

An unbiased coherence estimate, here called δ^{olk}, can be obtained by substituting in equations (28, 29) the correlation coefficient samples r_{XY} with the associated unbiased estimates $G(r_{XY})$. The precision of the unbiased estimate can be calculated using the Cramer-Rao lower band of equation (8).

In summary, the Olkin and Pratt estimator, established for real channel correlation, allows us to derive an unbiased coherence estimate for a target whose channel signals are jointly circular Gaussian distributed . This estimate δ^{okl} will be called "the Olkin coherence estimate". In contrast to the Siegert estimate d^{sig} of equation (18), δ^{okl} can be extended to non-Gaussian scenes whose backscattering satisfies the product model. In this case, equation (30), established under the Gaussian assumption, can be applied, and the unbiased estimate δ^{okl} can be used provided that the zero mean complex process components (I_k, and Q_k for $k = 1, 2$) satisfy the joint circular Gaussian conditions of equations (27).

4.3 Coherence magnitude estimation from (complex) coherence maps

4.3.1 The magnitude of the averaged sample coherence

The coherence estimate calculated from an L-look (complex) coherence map was defined in Section 4.1 as $\hat{D} = |\bar{\delta}_L|$ where $\bar{\delta}_L$ is the ML of $E(\delta_L)$. It was shown in Section 4.2.1 that the magnitude of the sample coherence expectation, $|E(\delta_L)|$, is practically unbiased for a relatively small number of looks $L \simeq 20$. These results can be extended to $|\bar{\delta}_L|$, and confirmed using the simulated offset SAR data (see Section 3.3) for a Gaussian scene. The L-look (complex) coherence map was calculated using equation (2) with $L \simeq 4$. $N \simeq 1000$ coherence samples were then averaged and the average magnitude $|\bar{\delta}_4|$ for different channel offsets was used to generate the speckle covariance function presented in Figure 4. $|\bar{\gamma}_4|$ is slightly biased even for low coherence, whereas the averaged sample coherence magnitude $\bar{d}_4$ is highly biased. The bias of $|\bar{\delta}_L|$ reduces with coarser resolution, and can be ignored for $L \simeq 20$ (for example, from Figure 5). For high resolution maps, the bias can be retrieved using the statistics of the L-look sample coherence δ_L. $E(\delta_L)$ is substituted with the estimate value $\bar{\delta}_L$ in equation (25), which is inverted to deduce an unbiased estimate of the coherence $\Delta = D\exp(j\beta)$, and consequently of its magnitude D and phase β.

The dispersion of the unbiased estimate $|\hat{\Delta}|$ can be calculated, as was done in Section 3.2. For a sufficiently large N value, $|\hat{\Delta}|$ is distributed normally about D with the variance $var_{CR}(|\hat{\Delta}|)/N$ (var_{CR} is

the Cramer-Rao lower bound of equation (8)), and the estimate confidence interval is:

$$CI = [\hat{\Delta} - z_c\sqrt{var_{CR}}(|\hat{\Delta}|)/\sqrt{N}, \hat{\Delta} + z_c\sqrt{var_{CR}}(|\hat{\Delta}|)/\sqrt{N}] \tag{31}$$

for a confidence level fixed by the confidence coefficient z_c.

The bias removal process using the statistics of the sample coherence can be performed on Gaussian scenes, as well as on those non-Gaussian scenes whose backscattering locally satisfies the product model (i.e. the texture parameter w has the same value for the two channels at each pixel averaged in the coherence estimate). This method is included in Figure 1 (a) as the "magnitude of the averaged sample coherence" method.

4.3.2 The magnitude of the averaged Olkin coherence estimate

Under the joint circular Gaussian assumption, the Olkin coherence estimate of equations (28) and (29) introduced in Section 4.3 may be used to generate an L-look coherence map. The averaged Olkin coherence estimate $\bar{\delta}_L^{olk}$ yields an unbiased estimate of the coherence whose magnitude and phase can be taken as the coherence parameter estimates. The dispersion of the magnitude coherence estimate $|\hat{\Delta}|$ can be calculated using the CR lower bound var_{CR}, as done above in equation (31).

This method is described in Figure 1 (b) as the "magnitude of the averaged Olkin estimate" method. The method can be extended to non Gaussian scenes whose backscattering locally satisfies the product model, provided that the joint circular Gaussian conditions of equation (27) are valid at each (L-look) pixel averaged in the coherence estimate $|\bar{\delta}_L^{olk}|$.

4.4 Implications for coherence magnitude estimation in stationary areas

The following points can be made for coherence estimation in stationary scenes:

- Spatial averaging in magnitude yields biased estimates $\bar{d}_L$, and $\bar{d}_L^{sig}$, whose bias can be removed as was shown in Section 3.
- The Siegert estimate $\bar{d}_L^{sig}$ does not yield an estimate of D in the presence of texture.
- Spatial averaging in complex is more efficient than spatial averaging in magnitude: it permits an immediate calculation of unbiased coherence magnitude estimates $|\bar{\delta}_L|$ (for L sufficiently value), and $|\bar{\delta}_L^{olk}|$.
- The sample coherence magnitude d_N method (described in section 2), which is more computationally efficient remains the preferred method for coherence estimation in stationary scenes.
- Unfortunately, this method is limited to stationary scenes, whereas the averaged sample coherence methods can be extended to certain nonstationary scenes, as shown below.

5 COHERENCE ESTIMATION IN NONSTATIONARY SCENES

5.1 Background

Coherence estimation was considered above in stationary scenes in which the processes (z_1, z_2, and $z_1 z_2^*$) involved in equation (1) are stationary (see Section 2.1). Such conditions are satisfied in homogeneous scenes, as well as in non-homogeneous scenes whose backscattering satisfies the product model. In the last case, the texture parameter w (defined in Section 2.3) which is channel independent, cancels out in equation (1), and the scene can be considered as stationary for coherence estimation.

In nonstationary areas, the processes (z_1, z_2, and $z_1 z_2^*$) involved in equation (1) might not be stationary in mean, and the sample coherence of equation (2) leads to a meaningless value, as was confirmed experimentally in [4]. In practice, stationarity in mean (the assumption that the mean $E(x)$ does not vary) may be relaxed: all that is required is that $E(x)$ does not change significantly within the observation interval [4, 13]. If such a condition is satisfied by each process involved in equation (1), the nonstationary processes can be considered locally stationary (named "stationary in increments" in [13]), and the coherence can be estimated over a moving stationary window. To characterize the spatially varying coherence, a new parameter should be defined as a function of the local coherence estimate.

5.2 Estimation of nonstationary coherence signals

The correlation function z_1 and z_2 at observation times $t_1 = t$ and $t_2 = t + \tau$ is:

$$R_{z1z2}(t, t+\tau) = E[z_1(t) z_2^*(t+\tau)] \tag{32}$$

The space- (or time-) averaged correlation function was introduced in [22] for nonstationary processes. It is given for finite power signals by [18, 22]:

$$\bar{R}_{z1z2}(\tau) = < R(t+\tau, t) >_t \tag{33}$$

where $< >_t$ indicates the space (or time) average operator:

$$< R(t+\tau, t) >_t = \lim_{T\to\infty} \frac{1}{2T} \int_{-T}^{T} R_{z1z2}(t, t+\tau) dt \tag{34}$$

Under the assumption that the limit $\bar{R}_{z1z2}(\tau)$ exists, the averaging process results in a stationary function $\bar{R}_{z1z2}(\tau)$, even though $R_{z1z2}(t_1, t_2)$ is nonstationary.

In the same way, the averaged coherence which corresponds to the normalized averaged correlation function can be defined. For zero channel time shift, and under the assumption that the limit $< \Delta(t, 0) >_t$ exists, the averaged coherence $\bar{\Delta}$ is:

$$\bar{\Delta} = < \Delta(t, 0) >_t \tag{35}$$

where $\Delta(t,\tau)$ is given by:

$$\Delta(t,t+\tau) = \frac{E[z_1(t)z_2^*(t+\tau)]}{\sqrt{E(|z_1(t)|^2)}\sqrt{E(|z_2(t+\tau)|^2)}} \tag{36}$$

The averaged coherence might be estimated by spatially averaging the coherence sample calculated over a moving window within which the processes can be assumed to be locally stationary. The averaged coherence estimate $\hat{\bar{\Delta}}$ is given by:

$$\hat{\bar{\Delta}} \;=\; \bar{\delta}_L \;\;=\;\; \frac{1}{N}\sum_{i=1}^{N}\delta_L^i \tag{37}$$

where L is the number of looks contained in the processing window, δ_L^i is the coherence estimate at the spatial position i, and N is the number of L-look coherence samples contained in the area under study. $\hat{\bar{\Delta}}$ of equation (37) is identical to the averaged sample coherence $\hat{\Delta}$ of equation (24) defined in section 4.1 for stationary processes. Hence, the averaged coherence magnitude $\bar{\delta}_L$ is suitable to estimate the coherence in stationary scenes, and in nonstationary scenes which are locally stationary. $|\bar{\delta}_L|$ provides an estimate of the magnitude of the averaged coherence: $|\bar{\delta}_L| = |\hat{\bar{\Delta}}|$. An estimate of the magnitude of the averaged coherence can also be obtained using the Olkin coherence estimate δ_L^{okl} of equation (28) under the local joint circular Gaussian assumption: $|\hat{\bar{\Delta}}| = |\bar{\delta}_L^{okl}|$.

In the same way, the space-averaged coherence magnitude $\bar{D}$ can be defined, and estimated as a function of the L-look sample coherence magnitude d_L of equation (3):

$$\hat{\bar{D}} \;=\; \bar{d}_L = \frac{1}{N}\sum_{i=1}^{N} d_L^i \tag{38}$$

$\hat{\bar{D}}$ of equation (38) is identical to the averaged sample coherence magnitude $\hat{D}$ of equation (22) defined in Section 3.2 for stationary processes. The averaged Siegert coherence magnitude $\bar{d}_L^{sig}$ (where d_L^{sig} is from equation (18)) can also be used as an estimate of the averaged coherence magnitude under the local joint circular Gaussian assumption: $\hat{\bar{D}} = \bar{d}_L^{sig}$.

5.3 Accuracy of the averaged sample coherence magnitude

For an area which contains n statistical ensembles, the $\bar{d}_L$ expectation is:

$$E(\bar{d}_L) \;=\; \frac{1}{n}\sum_{k=1}^{n} E(d_L^k)\;, \tag{39}$$

where $E(d_L^k)$ is the expectation of the L-look sample coherence magnitude for the k^{th} ensemble. If the sample magnitude coherence d_L^k of each ensemble k were unbiased, equation (39) would be equivalent to:

$$E(\bar{d}_L) \;\;=\;\; \hat{\bar{D}} \;\;=\;\; \frac{1}{n}\sum_{k=1}^{n} D^k \;\;, \tag{40}$$

where D^k is the coherence magnitude of the ensemble k, and $\bar{d_L}$ would yield an accurate estimate of the averaged coherence magnitude $\bar{D}$. Notice that for a stationary target, only one statistical ensemble exists, and the averaged coherence magnitude $\bar{D}$ is identical to the coherence magnitude D of the unique statistical ensemble: $\bar{D} = D$.

Under the assumption that the two channels are locally zero mean jointly Gaussian, the sample coherence magnitude statistics derived in Section 2 can be used. The fact that the sample coherence is generally biased (i.e $E(d_L)^k \neq D^k$), results in a biased estimate of $\bar{D}$. Since different ensembles are included in the averaged sample, the method described in Section 3.2 cannot be used to remove the estimate bias. The user must then confront the fact that the coherence is biased under low coherence conditions. Equation (6) can be used to fix the number of independent looks needed to obtain an insignificant bias for a coherence value larger than a given threshold, as done in [11, 21]. The same conclusion can be extended to the averaged Siegert estimate $\bar{d}_L^{sig}$ since d^{sig} is biased. If the region is not locally Gaussian, $\bar{d}_L^{sig}$ would yield to a different estimate than $\bar{D}$, as $E(d_L)^k \neq D^k$ for each ensemble k contained in the region of interest (see Sections 2.4 and 3.4).

5.4 Accuracy of the averaged complex coherence

The $\bar{\delta}_L$ expectation for an area which contains n statistical ensembles, is:

$$E(\bar{\delta}_L) \;=\; \frac{1}{n}\sum_{k=1}^{n} E(\delta_L^k) \tag{41}$$

where $E(\delta_L^k)$ is the expectation of the L-look sample coherence for the k^{th} ensemble. Under the assumption that the two channels are locally zero mean jointly Gaussian, the statistics of the sample coherence derived above (Section 4.2) can be used. For a sufficiently large L ($L \simeq 20$), the L-look sample coherence δ_L is practically unbiased and $E(\delta_L^k) = \Delta^k$ for each ensemble k. This leads to:

$$E(\bar{\delta}_L) \;=\; \hat{\bar{\Delta}} \;\;=\;\; \frac{1}{n}\sum_{k=1}^{n} \Delta^k \tag{42}$$

Notice that for a stationary target, only one statistical ensemble exists, and the averaged coherence $\bar{\Delta}$ is identical to the coherence Δ of the unique statistical ensemble: $\bar{\Delta} = \Delta$. An unbiased estimate of $\bar{\Delta}$ can also be obtained, under the local joint circular Gaussian assumption, with the averaged Olkin coherence estimate $\bar{\delta}_L^{olk} = \hat{\bar{\Delta}}$, as δ_L^{olk} is unbiased.

5.5 Implications for coherence estimation of "stationary in increments" signals

In contrast to the spatial averaging in magnitude, the averaging in complex permits the calculation of unbiased estimates $|\bar{\delta}_L|$ (for $L \geq 20$) and $|\bar{\delta}_L^{olk}|$ for the magnitude of the averaged coherence $|\bar{\Delta}|$. It is worth

noting that spatial averaging in magnitude yield (after bias removal) an estimate of the "incoherent" sum $\bar{D}$ (of equation (40), for n ensembles), whereas the averaging in complex leads to an estimate of the magnitude of the "coherent" sum $|\bar{\Delta}|$ (of equation (42)), which is generally of smaller value: $|\bar{\Delta}| \leq \bar{D}$. The last method, which permits the immediate calculation of an unbiased estimate, is preferred, provided that the user interest is the "coherent" sum $|\bar{\Delta}|$ and not the "incoherent" sum $\bar{D}$. In the case of a stationary coherence signal, the two methods estimate the same parameter $|\bar{\Delta}| = \bar{D} = D$, and the unbiased estimate $|\bar{\delta}_L|$ is again preferred to $|\bar{d}_L|$, which generally needs bias removal.

5.6 Estimation of the topographic phase corrected coherence in SAR interferometry

In certain non-homogeneous scenes, the processes involved in equation (1) cannot assumed to be stationary in increments, and the coherence cannot be estimated even locally. In some applications, the source of signal nonstationarity might be removed, and coherence can then be estimated. For example, in SAR interferometry, the nonstationarity of the cross-channel product $z_1 z_2^*$ is assigned to the phase changes due to topographic variations. The phase nonstationary is compensated at the spatial position i with a phase factor $\exp(-j\Phi_i)$ for the local imaging geometry, and the sample phase corrected coherence δ_{TPC} is used instead of the sample coherence δ of equation (2)[11]:

$$\delta_{TPC} = \frac{\sum_{i=1}^{L} z_{1i} z_{2i}^* \cdot \exp(-j\Phi_i)}{\sqrt{\sum_{i=1}^{L} |z_{1i}|^2} \sqrt{\sum_{i=1}^{L} |z_{2i}|^2}} \tag{43}$$

After phase compensation and under the assumption that the unique source of signal nonstationarity is the topographic phase variations, all the processes involved in equation (43) are stationary in the region of interest, and the channels can still be assumed to be zero mean jointly Gaussian. The results obtained in stationary regions with the sample coherence of equations (2), and (3) can then be extended to the modified sample coherence δ_{TPC}, and $d_{TPC} = |\delta_{TPC}|$. An unbiased estimate of the topographic phase corrected coherence magnitude $D_{TPC} = |\Delta|_{TPC}$ can be obtained using one of the unbiased methods described previously. Averaging in complex leads immediately to unbiased estimates whereas averaging in magnitude yields estimates which need bias removal. The sample coherence magnitude $|\delta_{TPC}|$ can also applied over the whole stationary (after topographic phase compensation) region of interest (see Section 2 for the sample coherence method). This method, which is less computationally expensive can be applied only if the topographic phase variations are well compensated. In the case of residual phase errors, the averaged sample coherence methods can be used as long as the signal can be assumed to be stationary in increments.

One might circumvent the nonstationarity problem related to the phase variations by eliminating the nonstationary phase term of $z_1 z_2^*$ in equation (1), and calculating the coherence of intensity channels (of equation (19)). This was done in [8] where the Siegert estimate was used for coherence magnitude

estimation. Note that the Siegert relationship of equation (18) was established for stationary processes. In the case of phase nonstationarity, the sample coherence magnitude d of equation (3) is meaningless, and the estimate obtained after bias removal (see section 3.4) is the averaged (square root of) correlation coefficient $\overline{R^{1/2}}$, given for an area of n statistical ensembles, by:

$$\overline{R^{1/2}} = \frac{1}{n}\sum_{k=1}^{n}\sqrt{R^k} \tag{44}$$

where R^k (from equation (17)) is the correlation coefficient of the statistical ensemble k. The parameter obtained in this way is different from the topographic phase corrected coherence magnitude D_{TPC}. Simulation were carried out in [2] to assess how different the two parameters $\overline{R^{1/2}}$, and D_{TPC} are. This problem is not discussed in this paper, and only the bias on the parameter which results from the estimation process, is discussed.

If the topographic phase does not change significantly within small areas, the coherence can be estimated locally using the sample coherence of equation (2), and the nonstationary coherence signal can be characterized with the space-averaged coherence. As explained above, the space averaging can be performed in magnitude to obtain a biased estimate of the incoherent sum $|\bar{D}|$ (of equation (40), for an area of n statistical ensembles), whose bias cannot be removed under low coherence conditions. The space averaging can also be performed in complex, and an unbiased estimate of the coherent sum $|\bar{\Delta}|$ (of equation(42)) is obtained. The two parameters $\bar{D}$, and $|\bar{\Delta}|$ used to characterize the nonstationary coherence signal are different: $\bar{D} \geq |\bar{\Delta}|$. If the nonstationarity of the coherence signal is associated only with the topographic phase change, the nonstationary coherence signal can be transformed to a stationary signal by compensating each sample coherence with a topographic phase term [11]. The spatial averaging in complex leads to an unbiased estimation of $|\bar{\Delta}_{TPC}|$ ($= |\Delta_{TPC}| = D_{TPC}$, as one ensemble is contained in the stationary scene after phase compensation) which is generally larger than the estimate $|\bar{\Delta}|$ obtained without phase compensation: $|\bar{\Delta}_{TPC}| \geq |\bar{\Delta}|$ (see [11]). Note that, in both the two cases, averaging in complex yields unbiased estimates of the two parameters $|\bar{\Delta}|$, and $|\bar{\Delta}_{TPC}|$. However, the precision of the estimate $|\hat{\bar{\Delta}}_{TPC}|$ obtained after removing the nonstationary phase should be better than the precision of $|\hat{\bar{\Delta}}|$ as all the samples belong to the same and unique statistical ensemble after phase compensation. The difference between the three parameters $\bar{D}$, $|\bar{\Delta}|$, and $|\bar{\Delta}_{TPC}|$ will not be discussed further in this paper.

6 EXAMPLES OF COHERENCE ESTIMATION: RESULTS AND DISCUSSION

The various methods presented in Figure 1 are illustrated using CCRS Convair-580 SAR HH-VV data [17]: two sets of calibrated complex data collected with the X- and C-band SAR polarimeters over a site at Wainwright, Alberta (X-band, 1989), and another at Altona, Manitoba (C-band, 1994). The first test scene described in [30] spans the incidence angle range 45°-69° and contains an old river bed, harvested alfalfa, wheat fields, and shrub-covered areas. The second test scene covers the incidence angle range 0°-50° and contains farm and urban areas.

The sample coherence magnitude d_N of equation (3) was calculated over large extended areas. Each area contains a sufficiently large number N of independent samples that the coherence magnitude estimate is essentially unbiased over stationary areas. The sample coherence magnitude is then calculated over (3x3, $L \simeq 4$) and (7x7, $L \simeq 20$) moving windows to generate 4-look and 20-look coherence magnitude and (complex) coherence maps. The averaged L-look magnitude coherence $\bar{d}_L$ (of equation (22)), and the magnitude of the averaged sample coherence $|\bar{\delta}_L|$ (of equation (24)) were calculated for the different samples selected on the coherence map. Table 1 presents the magnitude coherence estimates d_N and $\bar{d}_4$, as well as the sample standard deviation of d_4 measured from the 4-look coherence magnitude map. Equations (6) and (7) are used with the "unbiased" estimate values d_N obtained to calculate the multi-look coherence estimate mean $E(d_4)$ and standard deviation which can be expected. These values are presented in Table 1, as well as the error tolerance on the coherence magnitude estimates. Table 2 presents the results concerning $|\bar{\delta}_4|$ obtained from the 4-look (complex) coherence map, where equations (25) and (26) were used for the calculations related to the magnitude of the averaged 4-look sample coherence $|\bar{\delta}_4|$.

As can be seen for the selected stationary areas, the multi-look coherence estimates $\bar{d}_4$, and $|\bar{\delta}_4|$ measured on the 4-look coherence maps are very close to $E(d_4)$, and $|E(\delta_4)|$, respectively. This indicates that the bias can be removed accurately from the coherence magnitude estimates $\bar{d}_4$ and $|\bar{\delta}_4|$. Notice also the good agreement between the sample standard deviation measured from the 4-look coherence maps with the theoretical values. This good agreement with the theoretical statistics is confirmed for all of the observed areas whose backscattering satisfy the product model. For the nonstationary urban areas, the results differ between the three methods. The sample coherence magnitude yields erroneous results because of signal nonstationarity, and is disregarded. The two estimates $\bar{d}_4$ and $|\bar{\delta}_4|$ lead to different results since the two parameters to be estimated are different. The last method gives results close to zero because of the abrupt change of phase which is ignored in the magnitude method.

For the larger window of 7x7 ($L \simeq 20$), Table 3 presents the results obtained over the same areas. For the target with stationary coherence signal, the values obtained with the 20-look (complex) coherence

estimator $\bar{\delta}_{20}$, are very close to the coherence values obtained with the sample coherence magnitude. In practice, they do not need any bias removal. In contrast, the values obtained with $\bar{d}_{20}$ still need bias removal. For urban areas, the three methods again lead to different results for the reasons mentioned above. The results obtained with $\bar{\delta}_{20}$ should be unbiased whereas the ones obtained with $\bar{d}_{20}$ are biased (see Sections 3.2 and 4.3.1). Note the difference between the values obtained with $\bar{\delta}_{20}$ and $\bar{\delta}_4$. This difference may indicate that the coherence signal is not locally stationary over the 7x7 moving window (20-looks). Since the bias on $\bar{\delta}_4$ is practically insignificant for the actual low coherence value obtained (cf. Figure 5), the coherence estimate using the smallest window size (3x3) should be retained.

The results obtained under the joint circular Gaussian assumption with the averaged Siegert coherence magnitude estimate $\bar{d}_L^{sig}$ and the magnitude of the averaged Olkin coherence estimate $|\bar{\delta}_L^{olk}|$ over the 3x3 and 7x7 moving windows are presented in Tables 4 and 5, respectively. $\bar{d}_L^{sig}$ leads to biased estimates for all the samples under study. An unbiased estimate of D can only be deduced for Gaussian areas, as was explained in Section 3.4.

Considering the results presented in Table 5 for the the magnitude of the averaged Olkin coherence estimate $|\bar{\delta_L}^{olk}|$, it can be seen that the coherence values obtained with $L \simeq 4$ are biased. The joint circular Gaussian conditions (27) were then assessed. Neither condition was satisfied over the small 3x3 moving window. The differences between the terms on the right and the left sides of equations (27) are then significant, and equations (28) and (29) cannot be used for coherence estimation. For the larger window, the difference between the two terms becomes smaller and $|\bar{\delta}_{20}^{olk}|$ yields estimate values closer to the ones obtained with the estimate d_N. However, the results obtained with $|\bar{\delta}_{20}|$ are better. This indicates that the error due to the joint circular Gaussian assumption is still significant, and that these conditions need large areas to be satisfied. This limits the use of the coherence magnitude estimate $|\bar{\delta_L}^{olk}|$, which in addition consumes much more computing time than $\bar{d}_L$. The same conclusion can be extended to the Siegert estimate of equation (18).

Table 1: Coherence magnitude estimates from 4-look coherence magnitude map

	$\hat{D}$	$\bar{d}_4$	$E(d_4)$	$\sigma(d_4)$	$\sigma_t(d_4)$
River bed	0.319 ± 0.014	0.535 ± 0.015	0.518 ± 0.006	0.21	0.21
Harvested alfalfa	0.426 ± 0.016	0.587 ± 0.017	0.567 ± 0.006	0.21	0.20
Harvested wheat	0.599 ± 0.009	0.678 ± 0.011	0.666 ± 0.005	0.18	0.19
harv. alf.-wheat	0.516 ± 0.011	0.622 ± 0.012	0.618 ± 0.05	0.20	0.20
Shrub area 1	0.348 ± 0.013	0.552 ± 0.013	0.549 ± 0.005	0.21	0.21
Shrub area 2	0.482 ± 0.013	0.618 ± 0.014	0.606 ± 0.005	0.20	0.20
Bare field (scene 2)	0.799 ± 0.002	0.811 ± 0.003	0.817 ± 0.003	0.13	0.14
urban1 (scene2)	0.449 ± 0.004	0.525 ± 0.004	0.577 ± 0.003	0.31	0.21
urban2 (scene2)	0.294 ± 0.009	0.558 ± 0.008	0.507 ± 0.010	0.33	0.21

.

TABLE 2: Coherence estimates from 4-look (complex) coherence map

	$\hat{D}$	$\lvert\bar{\delta}_4\rvert$	$\lvert E(\delta_4)\rvert$	$\sigma(\delta_4)$	$\sigma_t(\delta_4)$
River bed	0.319 ± 0.014	0.282 ± 0.03	0.302 ± 0.008	0.50	0.47
Harvested alfalfa	0.426 ± 0.016	0.394 ± 0.037	0.407 ± 0.07	0.48	0.45
Harvested wheat	0.599 ± 0.009	0.577 ± 0.02	0.574 ± 0.007	0.40	0.36
harv. alf.-wheat	0.516 ± 0.011	0.491 ± 0.026	0.495 ± 0.05	0.43	0.42
Shrub area 1	0.348 ± 0.012	0.338 ± 0.032	0.346 ± 0.010	0.48	0.47
Shrub area 2	0.482 ± 0.013	0.464 ± 0.030	0.456 ± 0.006	0.46	0.47
Bare field (scene 2)	0.799 ± 0.002	0.775 ± 0.006	0.779 ± 0.003	0.27	0.29
urban1 (scene2)	0.449 ± 0.004	0.08 ± 0.009	0.427 ± 0.004	0.56	0.43
urban2 (scene2)	0.294 ± 0.009	0.03 ± 0.019	0.273 ± 0.010	0.60	0.47

.

TABLE 3: Coherence estimates from 20-look coherence maps.

	$\hat{D}$	$\bar{d}_{20}$	$\lvert\bar{\delta}_{20}\rvert$
River bed	0.319	0.377	0.309
Harvested alfalfa	0.426	0.455	0.419
Harvested wheat	0.599	0.612	0.589
mixture of harv. alf.-wheat	0.516	0.535	0.510
Shrub area 1	0.348	0.413	0.351
Shrub area 2	0.482	0.521	0.480
Bare field (scene 2)	0.799	0.804	0.794
urban1 (scene2)	0.449	0.380	0.130
urban2 (scene2)	0.294	0.395	0.07

.

TABLE 4: Coherence estimation using the averaged Siegert coherence magnitude estimate

	$\hat{D}$	$\bar{d}_4^{sig}$	$\bar{d}_{20}^{sig}$
River bed	0.319	0.551	0.410
Harvested alfalfa	0.426	0.610	0.433
Harvested wheat	0.599	0.679	0.620
mixture of harv. alf.-wheat	0.516	0.598	0.490
Shrub area 1	0.348	0.563	0.405
Shrub area 2	0.482	0.615	0.505
Bare field (scene 2)	0.799	0.788	0.821
urban1 (scene2)	0.449	0.539	0.376
urban2 (scene2)	0.294	0.580	0.479

.

TABLE 5: Coherence estimation using the magnitude of the averaged Olkin coherence estimate

	$\hat{D}$	$\lvert\bar{\delta}_4^{olk}\rvert$	$\lvert\bar{\delta}_{20}^{olk}\rvert$
River bed	0.319	0.268	0.303
Harvested alfalfa	0.426	0.380	0.436
Harvested wheat	0.599	0.538	0.574
mixture of harv. alf.-wheat	0.516	0.470	0.498
Shrub area 1	0.348	0.274	0.326
Shrub area 2	0.482	0.447	0.484
Bare field (scene 2)	0.799	0.764	0.793
urban1 (scene2)	0.449	0.076	0.129
urban2 (scene2)	0.294	0.068	0.111

7 CONCLUSION

In stationary regions, the sample coherence magnitude provides a coherence magnitude estimate which is asymptotically unbiased. For a finite number of samples N, the estimate d_N is biased mainly under low coherence conditions. The statistics of the sample coherence magnitude should be used to assess the accuracy and the precision of the estimate as a function of the number N of independent samples contained in the area of interest. The methods proposed in Section 2 can be used to remove the eventual bias, and to calculate the estimate precision. In nonstationary regions, the estimate leads to a meaningless value, and the sample coherence magnitude has to be calculated in small areas in which the original signals can be assumed stationary.

The space-averaged sample coherence magnitude $\bar{d}_L$ calculated from an L-look coherence magnitude map can characterize the coherence in certain nonstationary regions in which the original signals can be assumed stationary in increments. Averaging in magnitude yields an additional bias, and the estimate obtained is highly biased under low coherence conditions. A method is proposed for stationary regions to remove the bias, and to calculate the estimate precision as a function of the coherence map resolution (fixed by L), and the number N of averaged pixels. The bias cannot be removed in the nonstationary (stationary in increments) scenes, and the user should acknowledge the fact that the estimate is significantly biased mainly under low coherence conditions. The statistics of the sample coherence magnitude can be used to calculate the optimum coherence map resolution (number of looks L) to be used for unbiased coherence estimation within areas for which the coherence magnitude D is larger than a given threshold.

The coherence in nonstationary regions can also be characterized with the space averaged sample (complex) coherence. An unbiased coherence estimate $|\bar{\delta}_L|$ can be obtained for both stationary and nonstationary regions by spatially averaging the coherence map of sufficiently coarse resolution ($L \simeq 20$) in which the original signals can be assumed locally stationary. Averaging in complex is preferred to the averaging in magnitude provided that the user interest is the "coherent" sum $|\bar{\Delta}|$. If the "incoherent" sum $|\bar{D}|$ is required, $\bar{d}_L$ might be used with an eventual significant bias which cannot be removed under low coherence conditions.

Coherence estimation using approximate expressions obtained under the joint circular Gaussian assumption (such as the averaged Siegert estimate $\bar{d}_L^{sig}$, or the averaged Olkin estimate $|\bar{\delta}_L^{okl}|$) can only be applied on coarse resolution maps, since such an assumption needs large sample size to be realized. In this case, an unbiased coherence magnitude D can be obtained with $|\bar{\delta}_L^{okl}|$ in stationary and certain nonstationary scenes, whereas $\bar{d}_L^{sig}$ leads to a different parameter (than D) at the presence of texture.

ACKNOWLEDGMENT

The authors would like to thank Drs. R. Bamler (DLR), and K. Raney (The Johns Hopkins University) for interesting discussions, Drs. L. Gray, M. Lasserre, C. Livingstone (CCRS), and K. Mattar (Intermap) for their helpful comments on the manuscript. Comments and suggestions formulated by the anonymous reviewers were very helpful in completing the revised manuscript.

References

[1] M. Born and E. Wolf. *Principles of Optics: Electromagnetic Theory of Propagation, Interference and Diffraction of Light, Fifth Ed.* Pergamon Press, Elmsford, NY, 1985.

[2] P. B. G. Dammert. Accuracy of INSAR measurements in forested areas. In *Fringe'96 Workshop on ERS SAR Interferometry*, Remote Sensing Laboratories, University of Zurich, Switzerland, 30 Sept - 2 Oct, 1996. ESA SP-406, March 1997, pp. 37–49.

[3] S. L. Durden, J. J. van Zyl, and H. A. Zebker. The unpolarized component in polarimetric radar observations of forested areas. *IEEE Trans. Geoscience Rem. Sens.*, 28(2):268–271, 1990.

[4] M. R. Foster and N. J. Guinzy. The coefficient of coherence: Its estimation and use in geophysical data processing. *Geophysics*, XXXII(4):602–616, 1967.

[5] J. W. Goodman. Statistical analysis based on a certain multivariate complex Gaussian distribution (An introduction). *Ann. Math. Statis.*, 34(152):152–180, 1963.

[6] J. W. Goodman. *Statistical Optics.* John Wiley and Sons Inc., New York, 1984.

[7] I. S. Gradshteyn and I. M. Ryzhik. *Table of Integrals, Series, and Products.* Academic Press, San Diego, 1980.

[8] A. M. Guarnieri and C. Pratti. A quick and dirty coherence estimator for data browsing. *IEEE Trans. Geoscience Rem. Sens.*, 35(3):660–669, 1997.

[9] J. Hagberg. *Repeat-pass satellite SAR interferometry.* PhD thesis, Chalmers University of Technology, Göteborg, Sweden, Feb. 1994. Tech. Rep. No. 170L.

[10] J. O. Hagberg and L. M. H. Ulander. Calibration of interferometric SAR images. *EARSeL Adv. in Rem. Sens.*, 4(2):50–54, 1995.

[11] J. O. Hagberg, L. M. H. Ulander, and J. Askne. Repeat-pass SAR interferometry over forested terrain. *IEEE Trans. Geoscience Rem. Sens.*, 33(2):331–340, 1995.

[12] I. R. Joughin, D. P. Winebrenner, and D. B. Percival. Probability density functions for multi-look polarimetric signatures. *IEEE Trans. Geoscience Rem. Sens.*, 32(3):562–574, 1994.

[13] D.L.B. Jupp, A.H. Strahler, and C.E. Woodcock. Autocorrelation and regularization in digital images: basic theory. *IEEE Trans. Geoscience Rem. Sens.*, 26(4):463–473, 1988.

[14] M. G. Kendall and A. Stuart. *The Advanced Theory of Statistics, Vol. 1.* Griffin, London, 1963.

[15] J. S. Lee, K. W. Hoppel, S. A. Mango, and A. R. Miller. Intensity and phase statistics of multi-look polarimetric and interferometric SAR imagery. *IEEE Trans. Geoscience Rem. Sens.*, 32(5):1017–1028, 1994.

[16] F. K. Li and R. M. Goldstein. Studies of multibaseline spaceborne interferometric synthetic aperture radars. *IEEE Trans. Geoscience Rem. Sens.*, 28(1):88–97, 1990.

[17] C. E. Livingstone, A. L. Gray, R. K. Hawkins, P. W. Vachon, T. I. Lukowski, and M. LaLonde. The CCRS airborne SAR systems: Radar for remote sensing research. *Can. J. Rem. Sens.*, 21(4):468–491, 1995.

[18] S. N. Madsen. Spectral properties of homogeneous and nonhomgeneous radar images. *IEEE Trans. Aerospace Elect. Syst.*, AES-23(4):583–588, 1987.

[19] L. M. Novak, M. B. Sechtin, and M. J. Cardullo. Studies on target detection algorithms which use polarimetric radar data. *IEEE Trans. Aerospace Elect. Syst.*, AES-25(2):–, 1989.

[20] I. Olkin and J. W. Pratt. Unbiased estimation of certain correlation coefficients. *Ann., Math., Statist.*, 29:201–211, 1958.

[21] K.P. Papathanassiou, A. Reiger, and M. Coltelli. On the inteferometric coherence: a multifrequency and multitemporal analysis. In *Fringe'96 Workshop on ERS SAR Interferometry*, Remote Sensing Laboratories, University of Zurich, Switzerland, 30 Sept - 2 Oct, 1996. ESA SP-406, March 1997, pp. 319–330.

[22] A. Papoulis. *Probability, Random Variables and Stochastic Processes*. McGraw-Hill, New York, 1965.

[23] C. Prati and F. Rocca. Range resolution enhancement with multiple SAR surveys combination. In *Proc. 1992 International Geoscience and Remote Sensing Symposium (IGARSS'92), 26-29 May 1992, Houston, Texas, U.S.A.*, pages 1576–1578, 1992.

[24] S. Quegan and I. Rhodes. Statistical models for polarimetric data: consequences, testing and validity. *Int. J. Rem. Sens.*, 16(7):1183–1210, 1995.

[25] R. K. Raney. SAR response to partially coherent phenomena. *IEEE Trans. Antenna Propagat.*, AP–26(6):777–787, 1980.

[26] J. M. Rignot and J. J. van Zyl. Change detection techniques for ERS-1 SAR data. *IEEE Trans. Geoscience Rem. Sens.*, 31(4):896–906, 1993.

[27] M. S. Seymour and I. G. Cumming. Maximum likelihood estimator for SAR interferometry. In *Proc. 1994 International Geoscience and Remote Sensing Symposium (IGARSS'94), August 1994, Pasadena, U.S.A.*, pages 2272–2275, 1994.

[28] A. J. F. Siegert. . Technical Report 465, M.I.T. Rad. Lab., 1943.

[29] R. J. A. Tough, D. Blacknell, and S. Quegan. Estimators and distribution in single and multi-look polarimetric and interferometric data. In *Proc. 1994 International Geoscience and Remote Sensing Symposium (IGARSS'94), August 1994, Pasadena, U.S.A.*, pages 2176–2178, 1994.

[30] R. Touzi, C. E. Livingstone, J. R. C. Lafontaine, and T. I. Lukowski. Consideration of antenna gain and phase patterns for calibration of polarimetric SAR data. *IEEE Trans. Geoscience Rem. Sens.*, 31(6):1132–1145, 1993.

[31] R. Touzi and A. Lopes. Statistics of the Stokes parameters and of the complex coherence parameters in one-look and multi-look speckle field. *IEEE Trans. Geoscience Rem. Sens.*, 34(2):519–532, 1996.

[32] P. W. Vachon, J. A. Johannessen, and D. P. Browne. ERS-1 SAR images of atmospheric gravity waves. *IEEE Trans. Geoscience Rem. Sens.*, 33(4):1014–1025, 1995.

[33] S. H. Yueh, J. A. Kong, J. K. Jao, R. T. Shin, H. A. Zebker, and T. Le Toan. K-distribution and multi-frequency polarimetric terrain radar clutter. *J. Electromagnetic Waves Applic.*, 5(1):1–15, 1991.

Appendix 1: JOINT PDF OF THE COHERENCE AMPLITUDE AND PHASE

We use the same notation as [31]. $I_{kl} = \hat{j}_{kl}$ where $k, l = 0, 1$ and j_{kl} is an element of the coherence matrix $[J]$. The complex coherence is: $\delta = j_{12}/\sqrt{j_{11}j_{22}} = D\exp(j\beta)$. The complex coherence estimator is: $\hat{\delta} = I_{12}/\sqrt{I_{11}I_{22}} = d\exp(j\phi)$. Using the Wishart distribution [5], the joint pdf of the element I_{lj} can be written down [31]:

$$\begin{aligned} p(I_{11}, I_{22}, |I_{12}|, \phi) &= \frac{L^{2L}}{\pi\Gamma(L)\Gamma(L-1)} \frac{|I_{12}|(I_{11}I_{22} - |I_{12}|^2)^{L-2}}{|\det[J]|^L} \\ &\quad \exp\left[-L\left(\sigma_2^2 I_{11} + \sigma_1^2 I_{22} - 2D|I_{12}|\sigma_1\sigma_2\cos(\phi-\beta)\right)/\det[J]\right] \end{aligned} \tag{45}$$

If we introduce the variable $h = I_{11}I_{22}$, the following pdf can be deduced:

$$\begin{aligned} p(h, d, \phi) &= Kh^{L-1}d(1-d^2)^{L-2}\exp\left[\frac{2L\sigma_1\sigma_2 dD\sqrt{h}\cos(\phi-\beta)}{\det[J]}\right] \\ &\quad \cdot K_0\left(\frac{2L\sigma_1\sigma_2\sqrt{h}}{\det[J]}\right) \end{aligned} \tag{46}$$

where K_0 is the modified Bessel function, and K is a constant. To derive the joint pdf expression $p(d, \phi)$, equation (46) has to be integrated over h. The variable $u = \sqrt{h}$ is introduced, and the following integral analytical expression given in [7] is used:

$$\begin{aligned} \int_0^{+\infty} x^{\mu-1}\exp(-\alpha x)K_\nu(\beta x)\cdot dx &= \frac{\Gamma(\mu+\nu)\Gamma(\mu-\nu)}{\Gamma(\mu+0.5)} \frac{\sqrt{\pi}(2\beta)^\nu}{(\alpha+\beta)^{\mu+\nu}} \\ &\quad \cdot F\left(\mu+\nu, \nu+0.5; \mu+0.5; \frac{\alpha-\beta}{\alpha+\beta}\right) \end{aligned} \tag{47}$$

After some manipulations, the following expression is obtained:

$$\begin{aligned} p(d, \phi) &= \frac{(1-D^2)^L}{\pi\Gamma(L)\Gamma(L-1)} d(1-d^2)^{L-2}[\Gamma^2(L)F(L, L; 1/2, d^2D^2\cos^2(\phi-\beta)) + \\ &\quad 2\Gamma^2(L+1/2)dD\cos(\phi-\beta)F(L+1/2, L+1/2; 3/2; d^2D^2\cos^2(\phi-\beta))] \end{aligned} \tag{48}$$

Appendix2: EXPECTATION OF THE SAMPLE COHERENCE

$E(\delta)$ can be obtained from equation (48) by a double integration:

$$E(\delta) \;=\; \int_0^{2\pi}\int_0^1 d\exp(j\phi)p(d,\phi)d\phi\; dd \tag{49}$$

Equation (49) is first integrated over d. This leads to the following expression:

$$E(\delta) = \int_{\phi=0}^{2\pi}(J_1(\phi)+J_2(\phi))d\phi \tag{50}$$

where $J_1(\phi)$ is given by:

$$J_1(\phi) = \exp(j\phi)\frac{\Gamma(L)(1-D^2)^L}{4\sqrt{\pi}\Gamma(L+0.5)}\cdot_3 F_2(3/2,L,L;L+0.5,0.5;D^2\cos(\phi-\beta)^2) \tag{51}$$

and $J_2(\phi)$ is given by:

$$\begin{aligned} J_2(\phi) \;&=\; \frac{\Gamma^2(L+0.5)}{\pi\Gamma(L)\Gamma(L+1)}\exp(j\phi)D\cos(\phi-\beta)(1-D^2)^L \\ &\quad \cdot_3F_2(2,L+0.5,L+0.5;L+1,1.5;D^2\cos(\phi-\beta)^2) \end{aligned} \tag{52}$$

When integrated from 0 to 2π, $J_1(\phi)$ leads to a null expression. To calculate the integral of $J_2(\phi)$, the variable $x=\sin\phi$ is introduced and the following analytical expression derived in [7] is used:

$$\int_0^1(1-x)^{\mu-1}x^{\nu-1}\cdot_p F_q(a_1,..,a_p;b_1,..,b_q;ax)dx = \frac{\Gamma(\mu)\Gamma(\nu)}{\Gamma(\mu+\nu)}\cdot_{p+1}F_{q+1}(\nu,a_1,..,a_p;\mu+\nu,b_1,..,b_q;a) \tag{53}$$

After some manipulations, equation (25) is obtained.